INVESTIGATING AND MODELING OF THE MULTI-AXIAL FATIGUE AND COMPLEX DEFORMATIONS OF A NI-BASED SUPERALLOY FOR IMPROVING DISK LIFING

Xiaoguang Yang*, Duoqi Shi*， Hartmut Schlums, Wolfgang Rethkegel****
*** Beijing University of Aero. And Astro., PRC, **Rolls-Royce Deutschland, Germany**

Keywords: Constitutive Theory, Viscoplasticity, Multi-Axial Fatigue, Disk Lifing

Abstract

The research work in the paper aims to improve turbine disk lifing methodology by enabling viscoplastic constitutive models and utilizing multi-axial fatigue theory. A series of uniaxial and multi-axial (cruciform specimen) LCF tests, therefore, have been conducted under different cyclic loadings at high temperature to investigate the complex deformation and fatigue behaviors for Udimet 720 Li superalloy used in turbine disk. All its deformation behaviors, such as rate dependence, cyclic hardening, fast isotropic softening, mean stress relaxation and creep, are identified and used for viscoplastic modeling. The Bodner-Partom type viscoplastic constitutive model is adopted for that purpose. And it is modified to improve the modeling of the deformation behaviors, especially the behaviors under asymmetric cyclic loadings and dwell time. The constitutive models are implemented in general purpose FE software ABAQUS through UMAT interface combined with a self-adaptive time stepping strategy. The results show that improvements are very satisfactory.

By introducing a factor to consider creep damage effect on LCF, combined with the critical plane theory, a new multi-axial fatigue prediction method is proposed and verified based on the multi-axial fatigue results for different loadings conditions. Meanwhile, four common-used multi-axial fatigue theories are used for the comparisons; the predicted results show that the scatter band is in ± 2 times, which are much better than the results by other four theories.

1 Introduction

Aero-engine Turbine disc lifing methodology is an essential part in the design of reliable, competitive, efficient and safe jet engines. Conventional lifing methods assume that damage occurs in the low-cycle fatigue region, and other damage phenomena such as creep are covered by global consideration. But the interaction of non-linear effects like creep and plasticity has a greater influence on component life, especially under multiaxial loadings with dwell time. That makes the increasing needs for getting more understanding and accurate modelling of the complex deformation and failure behaviours under such situations. According to the recent developments of multi-axial fatigue and viscoplastic constitutive theories, based on the results of uniaxial and multi-axial LCF tests with or without dwell time, a modified Bodner-Partom type viscoplastic constitutive model was developed for improving the modelling of the complex deformation behaviours. And a creep-damage-coupled and critical-plane-based multi-axial fatigue method was proposed to improve the aero-engine turbine disc lifing.

2 Uniaxial and Multiaxial Tests

The material in the tests is Udimet 720 Li Ni-based superalloy, normally used for turbine disk. At first, the uniaxial tests are carried out by utilizing normal smooth-bar specimen, which consists of five types of loadings:

1) Monotonic loadings with different strain rates (10^{-2},10^{-3},10^{-4}).
2) Symmetrically cyclic strain-controlled loadings (Rε=-1).
3) Asymmetrically cyclic strain-controlled loadings (Rε=0).
4) Creep
5) Asymmetrically cyclic stress-controlled loadings (Rσ=0) with hold time in tensile peak (1 sec. and 120 sec.)

The test aim is to investigate the complex mechanical and fatigue behaviours of Udimet 720 Li under the typical loading conditions of turbine disk, such as rate-dependent monotonic tension, creep, cyclic hardening and mean stress relaxation, creep-fatigue interaction, etc. The first four tests are used for both viscoplastic constitutive modelling and fatigue modelling. They are also used to identify the material parameters. And the last test is used for verifying the constitutive models.

Multi-axial LCF tests were carried out by using cruciform specimen. The cyclic loading types (Rσ=0.1) include bi-axial and combined loadings. Totally, 17 uniaxial LCF tests and 23 cruciform multi-axial LCF tests were finished. Meanwhile a few creep tests were conducted under different stresses. The fractured cruciform specimen is showed in Fig.1. All test works are done in RRD.

Fig.1 Fractured Cruciform Specimen

The test temperatures are 650℃, 675℃ and 700℃. The uniaxial tests are mainly focused on 650℃ and 700℃, and multi-axial tests are mainly on 675℃.

3 Viscoplastic Constitutive Modeling of Complex Deformations

3.1 The Bodner-Partom Constitutive Theory and Its Modeling

The accurate stress and strain calculations are vital for accurate life predictions. Due to inherent complexity of deformations of turbine components under working conditions, classic elastic-plastic and creep theories seem to not have such capabilities. But the viscoplastic constitutive model is promising one. In the past three decades, based on thermodynamics and dislocation dynamics, a variety of viscoplastic constitutive theories have been developed and evaluated for dealing with such problems. Their advantages are that all observed mechanical responses could be treated as a result of the same internal physical processes. Therefore, single or multiple internal variables could be used to represent time-dependent and time-independent inelasticity. The evolutionary equations of the internal state variables are based on their microstructure variation, which are regarded as being a better approach of the governing physical processes than the classic plastic constitutive theories for those complex deformation behaviors, especially for the deformations under asymmetrically cyclic loadings.

Here, we have chosen the Bodner-Partom unified viscoplastic constitutive equations (B-P model) for that purpose because of its simplicity and clarity, which mainly utilized one internal variable. Normally, that internal variable consists of two parts: one is isotropic part, and another is kinematic part in order to consider short-range and long-range effects on deformations, respectively. B-P model has no yielding criterion. Its original forms are given in [1,2,3] as the following:

$$\dot{\boldsymbol{\varepsilon}}_{ij} = \dot{\boldsymbol{\varepsilon}}^{e}_{ij} + \dot{\boldsymbol{\varepsilon}}^{in}_{ij} \tag{1}$$

$$\dot{\varepsilon}^{in}_{ij} = D_0 \exp\left[-\frac{1}{2}\left(\frac{\left(Z^I + Z^D\right)^2}{3J_2}\right)^n\right]\frac{S_{ij}}{J_2} \tag{2}$$

$$\dot{Z}^I = m_1\left[Z_1 - Z^I(t)\right]\cdot\dot{W}^p(t) - A_1 Z_1\left[\frac{Z^I(t) - Z_2}{Z_1}\right]^{r_1} \quad (3)$$

$$Z^D(t) = \boldsymbol{\beta}_{ij}(t)\mathbf{u}_{ij}(t) \quad (4)$$

$$\dot{\boldsymbol{\beta}}_{ij}(t) = m_2\left[Z_3\mathbf{u}_{ij}(t) - \boldsymbol{\beta}_{ij}(t)\right]\cdot\dot{W}_p - A_2 Z_1\left[\frac{(\boldsymbol{\beta}_{kl}\boldsymbol{\beta}_{kl})^{1/2}}{Z_1}\right]^{r_2}\mathbf{v}_{ij} \quad (5)$$

$$\mathbf{u}_{ij}(t) = \frac{\boldsymbol{\sigma}_{ij}(t)}{(\boldsymbol{\sigma}_{kl}\boldsymbol{\sigma}_{kl})^{1/2}}\ ; \qquad \mathbf{v}_{ij}(t) = \frac{\boldsymbol{\beta}_{ij}(t)}{(\boldsymbol{\beta}_{kl}\boldsymbol{\beta}_{kl})^{1/2}} \quad (6)$$

Here, $\dot{W}_p = \sigma_{ij}\dot{\varepsilon}_{ij}^{in}$ is the inelastic work rate. The initial conditions: $Z^I(0) = Z_0$ and $\beta_{ij}(0) = 0$. D_0, Z_0, Z_1, Z_2, Z_3, m_1, m_2, n, A_1, A_2, r_1, r_2 are material parameters. Concerning their identification and optimization, please refer to the article [4]. One point is worth noting that the optimized parameters obtained from cyclic deformation curves are usually spoiled during the optimizations for creep. So, a hierarchical optimization strategy is needed. For Udimet 720Li, the material parameters at 650℃ and 700℃ are obtained, and the parameters of 675℃ are interpolated between that of two temperatures

The calculated results by the original B-P model are shown from Fig. 2 to Fig.6. Because of space limitation, the only results at 650℃ are given as the examples.

It was found that the original B-P model was not able to model all cyclic behaviors accurately, especially for the early reversing yielding (fast isotropic softening) and mean stress relaxation under R=0 loadings as shown in Fig. 3 and 4 although it can model cyclic hardening of R=-1 cyclic loadings well [5 , 6]. In general, the kinematic hardening variable is attributed to be the primary reason for such phenomena (ratcheting or mean stress relaxation) and needs be developed further [7]. One modification of the model was made in [3, 8 , 9] where the parameters m_1 and m_2 in equation (3) and (5) are considered to be the functions of isotropic and kinematic hardening, respectively. However, it is still unable to model ratcheting and mean stress relaxation. So, more works should be done for the modification.

3.2 Modification of B-P Model For Improving The Modeling of Cyclic Behaviors

The motivation for improving the modeling mainly stems from two sides. The first is on the basis of the assumption of three stages work-hardening, easy, linear and parabolic slip, according to P. Feltham's work [10]. So, the hardening variable Z^I and Z^D could be divided into three parts respectively.

$$Z^I = \sum_{k=1}^{3} Z_k^I \ ; \ Z^D = \sum_{k=1}^{3} \beta_{ij}^{(k)} u_{ij} \quad (7)$$

The second is the modification of Armstrong-Frederich's nonlinear hardening rules as done by Ohno and Wang [11,12] to Chaboche viscoplastic theory for modeling ratcheting. Therefore, the hardening rules of the kinematic variables in equation (7) are reformulated as:

$$\dot{\boldsymbol{\beta}}_{ij}^{(k)} = m_k\left[D_k\mathbf{u}_{ij} - \left|\frac{J(\boldsymbol{\beta}^{(k)})}{D_k}\right|^{f_k}\boldsymbol{\beta}_{ij}^{(k)}\right]\dot{W}^p - A D_k\left|\frac{J(\boldsymbol{\beta}^{(k)})}{D_k}\right|^{r}\mathbf{v}_{ij}^{(k)}, k = 1,2,3 \quad (8)$$

with $\beta_{ij}^{(k)}(t=0) = 0$ and $J(\beta^{(k)}) = (\beta_{lm}^{(k)}\beta_{lm}^{(k)})^{1/2}$. Then,

$$\dot{Z}_k^I = l_k\left[H_k - Z_k^I(t)\right]\dot{W}^p - AH_k\left|\frac{Z_k^I(t) - C_k}{H_k}\right|^r, k = 1,2 \quad (9)$$

$$\dot{Z}_3^I = l_3\left[H_3 - \left|\frac{Z_3^I}{H_3}\right|^{f_4} Z_3^I\right]\dot{W}^p - A\cdot H_3\left|\frac{Z_3^I}{H_3}\right|^r \quad (10)$$

With initial condition: $Z_k^I(0) = H_{0k}$, H_{0k}(k=1,2,3) are temperature-dependent material parameters. In fact, the third isotropic hardening variable was introduced only for considering early-reverse yield (or fast isotropic hardening) during unloading particularly for Udimet 720 Li material.

Totally, there are 26 parameters included in the modified model: E, n, D_0, A, r $\{H_k, l_k, C_k, H_{0k}, m_k, D_k, f_k, (k = 1,2,3)\}$. Here, H_k, l_k, C_k, H_{0k}, D_k, m_k, has the same physical meanings as Z_1, m_1, Z_2, Z_0, Z_3, m_2 of the original

B-P model, respectively. For simplicity, we can set $C_k = H_{0k}$. If only monotonic loading and creep loading are concerned, the parameters taking effect could be greatly reduced by setting l_k , m_k (k=2,3) and f_k (k=1,2,3) equal to zero. Again, as done for original B-P model, the same methodology for identifying and optimizing the material parameters is adopted based on Levenberg-Marquadt algorithm. The parameters can be used to simulate time-independent plasticity and time-dependent creep simultaneously. Table1 lists the parameters only at 650℃.

To enable the numerical calculation of real components, both the original and modified B-P constitutive models were implemented into ABAQUS through UMAT using a self-adaptive explicit time stepping strategy for the numerical integration of a constitutive equation.

Table 1 The material parameters of the modified model at 650℃

l_1, MPa^{-1}	l_2, MPa^{-1}	l_3, Mpa^{-1}	H_{01}, MPa	H_{02}, MPa	H_{03} MPa
0.0217	12.95	4.116	11.9	643.7	0
H_1 MPa	H_2 MPa	H_3 MPa	D_1 MPa	D_2 MPa	D_3 MPa
147.1	1794.6	-496.1	133.7	246.6	493.1
m_1, MPa^{-1}	m_2, MPa^{-1}	m_3, MPa^{-}	f_1	f_2	f_3
7.58	0.1448	1.782	0.88	1.7	1.0
n	r	A, Sec^{-1}	E,MPa		
2.62	0.7	4.0e-5	195196.5		

The increased numbers of internal variables do allow much more flexibility in representing the viscoplastic, time- and temperature-dependent response. Fig.3, Fig.4 and Fig. 6 show its big improvements in modelling typical steady stress-strain loops, mean stress relaxation and stress-strain curves under stress-controlled LCF loading with tensile dwell time 1 second.

Finally, in order to improve the modeling of creep of the third period, the classic Rabotnov-creep-damage equation was adopted to be coupled with the modified B-P model.

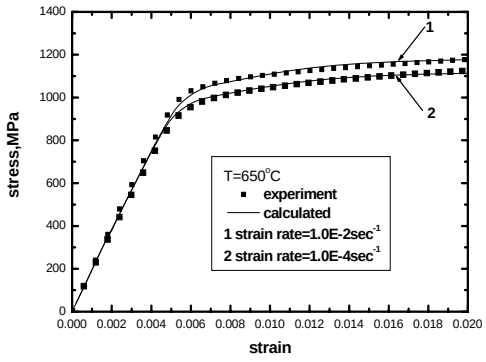

Fig.2 The Calculated monotonic tensions

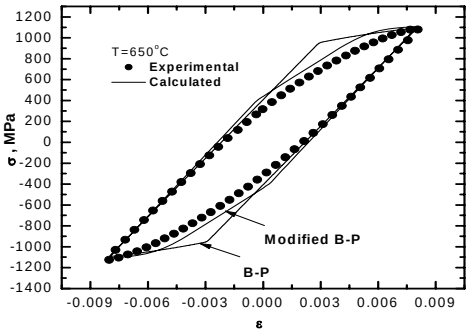

Fig.3 Calculated and experimental result of hysteresis loop under symmetric cyclic loading

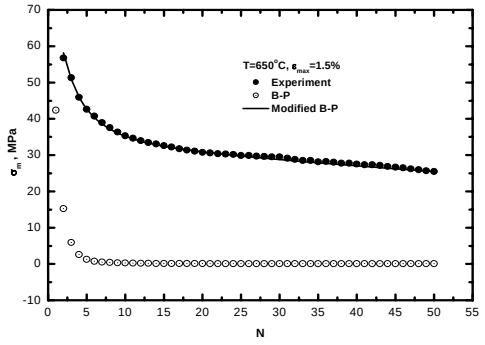

Fig.4 Calculated mean stress relaxation curve compared with the experimental result

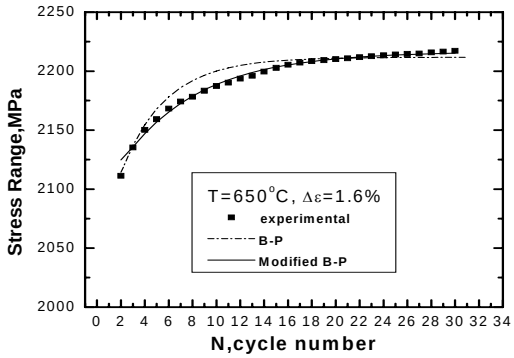

Fig.5 Calculated and experimental results of cyclic hardening curve

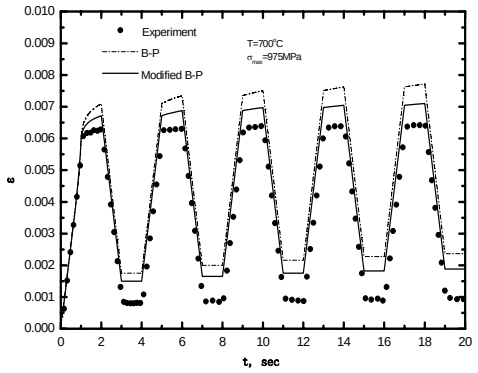

Fig.6 Calculated strain evolution under stress controlled asymmetric cyclic loading (Rσ=0)

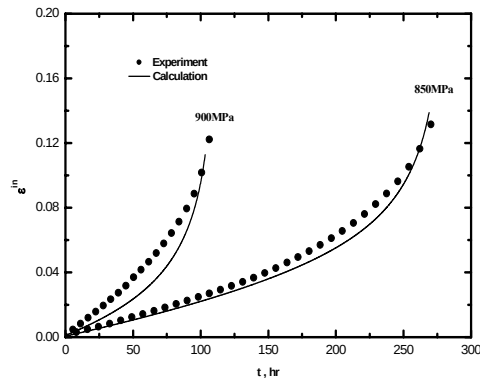

Fig.7 Calculated creep curves (considering the damage-effect in the third period of creep).

4 High Temperature Multi-axial Fatigue Modeling

4.1 Multi-axial LCF Model

Although a lot of multi-axial fatigue models were developed for different considerations, the critical-plane-based method is thought as a promising one. Differences between models are to use different damage parameters to define the critical plane on which damage has the maximum value. The four existed models were evaluated in the present study. These included Fatemi-Socie (FS) [13], Smith-Watson-Topper (SWT) [14], Glinka (GLK) [15] and Chu-Conle-Bonnen (CCB) [16] parameters.

The FS parameter was calculated using the maximum shear strain amplitude, $\Delta\gamma_{max}/2$, and the maximum normal stress, σ_{max}, on the critical plane:

$$FS = \frac{\Delta\gamma_{\max}}{2}(1 + k\frac{\sigma_{n,\max}}{\sigma_y}) \qquad (11)$$

Where, σ_y is the yield strength and k is a fitting parameter. In the present study, k=1, was used.

The SWT parameter was calculated using the maximum normal strain amplitude, $\Delta\varepsilon_{max}/2$, and the maximum stress, σ_{max}, on the critical plane:

$$SWT = \frac{\Delta\varepsilon_{\max}}{2}\sigma_{n,\max} \qquad (12)$$

The Glinka parameter was calculated as the sum of two products: (1) the product of the maximum shear strain amplitude, $\Delta\gamma_{max}/2$ and the maximum shear stress amplitude, $\Delta\tau_{max}/2$; (2) the product of the maximum normal strain amplitude,$\Delta\varepsilon_{max}/2$ and the maximum normal stress amplitude, $\Delta\sigma_{max}/2$, on the critical plane:

$$GLK = \frac{\Delta\gamma_{\max}}{2}\frac{\Delta\tau_{\max}}{2} + \frac{\Delta\varepsilon_{\max}}{2}\frac{\Delta\sigma_{\max}}{2} \qquad (13)$$

The CCB parameter was also calculated as the sum of two products: (1) the product of the maximum shear stress, $\Delta\tau_{max}$ and the maximum shear strain amplitude, $\Delta\gamma_{max}/2$; (2) the product of the maximum normal stress, $\Delta\sigma_{max}$ and the maximum normal strain amplitude, $\Delta\varepsilon_{max}/2$

$$CCB = (\tau_{\max}\frac{\Delta\gamma_{\max}}{2} + \sigma_{\max}\frac{\Delta\varepsilon_{\max}}{2}) \qquad (14)$$

The critical plane could be determined by scanning through all the computed stresses and strains at all the time steps of the fatigue cycle according a search algorithm in [17].

In the research, in order to include creep damage effect under R=0.1 cyclic loadings with holding time in tensile peaks. A factor k*, called a Creep-Fatigue-Interaction factor, was defined as the following

$$k^* = 1 + \left(t_d^t / t_R^t + t_d^c / t_R^c\right) N_f \qquad (15)$$

Here, t_R^t and t_R^c are rupture times corresponding to the applied stresses under the tensile peak and compressive peak, respectively.

t_d^t and t_d^c are dwell times corresponding to tensile peak and compressive peak, respectively. The physical meaning of k^* roots from the general understanding for creep damage yielded by hold load during dwell time.

Based on the observation for biaxial fracture mode of cruciform, the crack initiation is viewed as on the critical plane defined by the maximum amplitude of normal strain, and the maximum stress on the normal direction of the plane enhances the crack propagation. Hence, we define an energy–type fatigue damage parameter $(\sigma_{\max}\Delta\varepsilon/2)^{k^*}$, and proposed the following equation to model multi-axial fatigue:

$$(\sigma_{\max}\Delta\varepsilon/2)^{k^*} = A(2N_f)^m + B(2N_f)^n \qquad (16)$$

J. Zrnik et al [18] reported the relationship of material deformation, fatigue life with micro structural evolution during fatigue-creep process of Ni-based superalloy. They found that fatigue life is strongly dependent on dwell time and that nonlinear relation exists between dwell time and cyclic number of fracture. It means that the creep damage introduced by dwell time has strong coupling with the fatigue damage in every cycle, which induces nonlinearity between total damage and dwell time. The CFI factor we introduced is attempted to acts as index to characterize such nature.

4.2 FE Analysis of Cruciform Specimen

The FE model of one-eighth cruciform specimen under biaxial LCF loading is shown in Fig. 8. The stress and strain histories for each loading condition are calculated by the developed UMAT combined with ABAQUS.

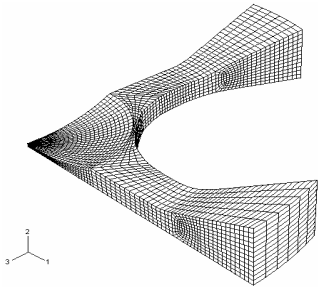

Fig.8 FE model of cruciform (loading along axial 1 and 3)

Fig. 9 shows part of the computed stress and strain history at the centre of cruciform (most damage location). The results show that both mean stress relaxation and ratcheting have occurred.

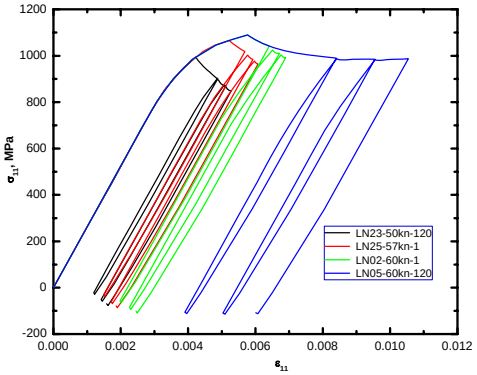

Fig.9 Simulated stress-strain loops for cruciform under equal-biaxial LCF loading at 650 ℃ with tensile dwell time 1s and 120s.

4.3 Biaxial LCF Life Prediction of Cruciform

Based on fatigue life data and FE analysis results, the high temperature multi-axial fatigue life can be predicted for each loading case using both the given life equation (16) and other four equations combined with he critical plane idea. The results are shown from Fig.10 to Fig.14.

It can be known that all four normal multi-axial fatigue models exhibit over 100 times scatter band. The models, therefore, seem to be questionable when used for disk lifing. One of reasons should be that these models do not consider the effect of dwell time and the interaction of creep and fatigue on multi-axial fatigue life.

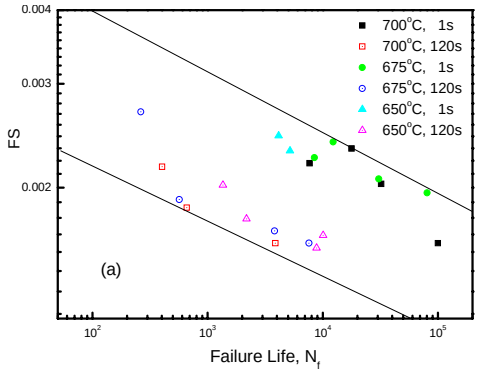

Fig.10 Life prediction by FS model

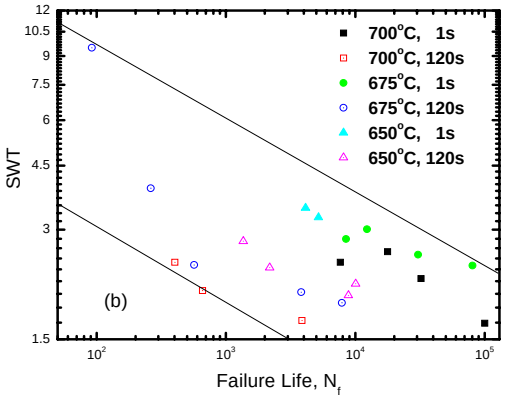

Fig.11 Life prediction by SWT model

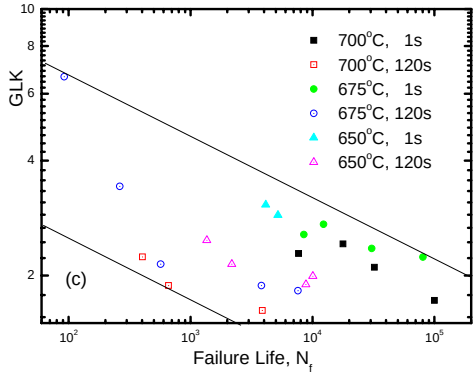

Fig. 12 Life prediction by GLK model

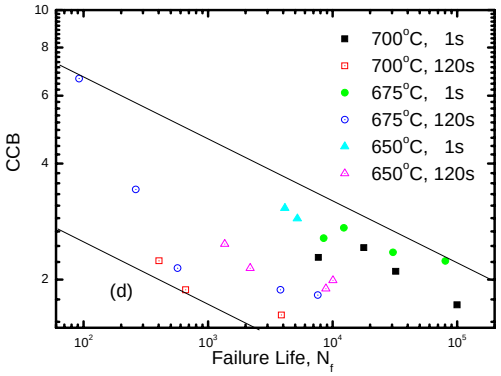

Fig.13 Life prediction by CCB model

Equation (16) can be looked as a modification to the existing critical-plane-based multi-axial fatigue models by use of the factor, k^*, to characterize the effect of dwell time on fatigue failure that is not considered in the above models. The constants, A, m, B and n in equation (16) are considered as material-dependent constants and are independent of temperature and loading in present study. For Udimet 720Li, these constants are fitted from uniaxial LCF life data are: A=20.37, B =3.32, m=n=-0.191.

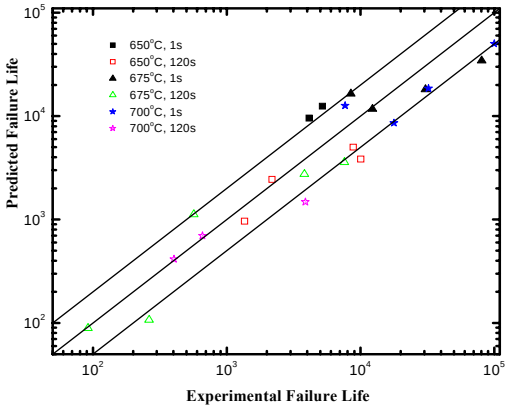

Fig.14 The predicted and experimental Bi-axial LCF life by The Equation (16)

Fig.13 shows that the scatter band by the new fatigue model is within ±2 times for all results including different temperatures and dwell times. It indicates that the model is the best for the present fatigue data of the superalloy. At the same time, life modeling of uniaxial fatigue data is also good within a factor of two. The validity of life prediction for both uniaxial and biaxial fatigue data reveals that the model is reasonable for fatigue with dwell time at elevated temperature.

5 Summary and Conclusion

Based on the experiment results of a superalloy Udimet 720 Li under uniaxial cyclic loadings at high temperature, its complex deformation behaviors are identified and used for constitutive modeling. The special concerns are focused on the deformation behaviors under asymmetric cyclic loading, such as mean stress relaxation, creep-fatigue interaction and simultaneous simulation of cyclic plasticity and creep. The B-P type viscoplastic constitutive model is used and modified for that purpose based on the ideas proposed by Ohno and Wang for the Chaboche viscoplastic constitutive model. The results show that the modified B-P model can largely improve the capabilities simulating the complex deformations at high temperature.

The high temperature multi-axial LCF tests utilized the cruciform specimen have been

conducted under biaxial loadings and combined loadings to understand the multi-axial fatigue failure behaviors. The dwell time effect is a main concern in establishing a new multi-axial LCF prediction method. So, the creep-fatigue factor is introduced and combined with the critical plane idea. The equation (16), the new multi-axial fatigue life prediction method, has given the better predicted results compared with four normal multi-axial theories. Finally, we think that the new multi-axial fatigue life prediction method combined with the viscoplastic constitutive theory is promising to improve turbine disk lifing methodology.

References

[1] Bodner, S. R., Partom, Y. Constitutive Equations for Elastic-Viscoplastic Strain Hardening Materials. *ASME J. Appl. Mech*. 42, 385-389, 1975.

[2] Rowley, M. A., Thornton, E. A. Constitutive Modeling of the Visco-Plastic Response of Hastelloy-X and Aluminum Alloy 8009. *ASME J. Eng. Mat. Tech.* Vol. 118, pp 19-27, 1996.

[3] Bodner, S. R., Lindenfeld, A., Constitutive modeling of the stored energy of cold work under cyclic loading. *European Journal of Mechanics /A*, Vol. 14, No.3, pp 333-348, 1995.

[4] SHI Duo-qi, YANG Xiao-guang, WANG Yan-rong. Constitutive modeling of hardening and creep response of a Nickel-based super-alloy Udimet720Li . *Chinese Journal of Aeronautics*, Vol. 16, No.3, pp 187-192, 2003.

[5] Ramaswamy,V.G. A constitutive model for the inelastic multiaxial cyclic response of a nickel base superalloy Rene 80, *NASA-CR-3998*, 1986.

[6] Stouffer, D. C. and Dame, L. T. *Inelastic Deformation of Metals*, John Wiley & Sons, Inc., 1996.

[7] Bari, S., and Hassan, T. Anatomy of coupled constitutive models for ratcheting simulation, *International Journal of Plasticity*, Vol. 16, pp 381-409, 2000.

[8] Khen, R., Rubin, M. B., Analytical modeling of second order effects in large deformation plasticity. *Int. J. Solids Structures*, Vol. 29, No.18, pp 2235-2258, 1992.

[9] Kroupa, J. L., Bartsch, M. Influence of viscoplasticity on the residual stress and strength of a titanium matrix composite after thermomechanical fatigue. *Composites Part B*, 29B, pp 633-642 , 1998.

[10] Feltham, P., *Hardening of Metals*, Freund Publishing House, 1980.

[11] Ohno, N., and Wang, J.D. Kinematic hardening rules with critical state of dynamic recovery, Part Ⅰ and Ⅱ. *Int. J. of Plasticity*, Vol. 9, pp 375-390, pp 391-403, 1993.

[12] Ohno, N., Constitutive Modeling Of Cyclic Plasticity With Emphasis On Ratchetting, *Int. J. of Mech. Sci.* , Vol. 40, Nos. 2-3, pp 251-261, 1998.

[13] Fatemi, A., and Socie, D.F. A critical plane approach to multiaxial fatigue damage including out-of-phase loading, *Fatigue and Fracture of Engineering Materials and Structures*, Vol. 11, No.3, pp 149-166, 1988.

[14] Smith, R.N., Watson, P., and Topper ,T.H. A Stress-Strain Function for the Fatigue of Metals, *Journal of Materials, JMLSA,* Vol. 5, pp 767-778, 1970.

[15] Glinka G, et al. A multiaxial fatigue strain energy density parameter related to the critical fracture plane. *Fatigue and Fracture of Engineering Materials and Structures,* Vol. 18, No.1, pp 37-46, 1995.

[16] Chu, C. C. Fatigue damage calculation using the critical plane approach. *Journal of Engineering Materials and Technology,* Vol. 117, pp 41-49, 1995.

[17] Das, J., Sivakumar S.M. An evaluation of multiaxial fatigue life assessment methods for engineering components, *International Journal of Pressure Vessels and Piping,* Vol. 76, pp 741–746, 1999.

[18] Zrnik,J.,et al. Influence of hold period on creep–fatigue deformation behaviour of nickel base superalloy. *Materials Science and Engineering,* A319–321, pp 637–642, 2001.